

large broadening (FWHM 290 meV) to which the inhomogeneous distribution of the dot sizes strongly contributes (~170 meV). Additionally, the luminescence is expected to be broadened by electronic states as a result of a high density of ion-induced surface defects of these uncovered dots, seen in the HTEM image (Fig. 3) as a ~2-nm-thick amorphous layer.

With respect to the potential of this technique for device fabrication, ion-induced defects have to be considered. These defects are sources for nonradiative recombination and therefore strongly deteriorate the optical and electrical properties. They must be reduced before devices can be fabricated. Possible methods are chemical etching, annealing, surface passivation, and overgrowth of the dots, methods which are performed ideally in situ. Overgrowth of the dots appears feasible because they exhibit a thermal stability up to 450°C.

The demonstration of regular dot formation on GaSb surfaces presented here may lay ground to extend the theory for ripple formation to normal incident ion sputtering. The formation mechanism for the nanometer-scaled dots relies only on the sputtering process and the diffusive transport on surfaces; therefore, we conclude that this mechanism should be universal and transferable to other materials. This conclusion is supported by experiments on InSb and Ge where the same dot formation as reported here for GaSb was observed (16). The successful demonstration of dot formation on Ge may open the way to produce nanostructures on the technologically important group IV semiconductor materials. The technical application of the produced nanostructures could include quantum dots for quantum devices and for black surfaces for optoelectronic and photovoltaic applications.

References and Notes

1. G. Springholz, V. Holy, M. Pinczolis, G. Bauer, *Science* **282**, 734 (1998); E. R. Glaser, B. R. Bennett, B. V. Shanabrook, R. Magno, *Appl. Phys. Lett.* **68**, 3614 (1996); M. Grundmann *et al.*, *Phys. Rev. Lett.* **74**, 4043 (1995).
2. S. Facsko *et al.*, patent pending.
3. G. Carter, B. Navinšek, L. Whitton, in *Sputtering by Particle Bombardment II*, vol. 64 of *Topics in Applied Physics*, R. Behrisch, Ed. (Springer-Verlag, New York, 1991), pp. 231–269.
4. E. Chason *et al.*, *Phys. Rev. Lett.* **72**, 3040 (1994).
5. T. M. Mayer, E. Chason, A. J. Howard, *J. Appl. Phys.* **76**, 1633 (1994).
6. G. Carter and V. Vishnyakov, *Phys. Rev. B* **54**, 17647 (1996).
7. S. Rusponi, C. Boragno, U. Valbusa, *Phys. Rev. Lett.* **78**, 2795 (1997); S. Rusponi, G. Constantini, C. Boragno, U. Valbusa, *ibid.* **81**, 4184 (1998).
8. R. M. Bradley and J. M. E. Harper, *J. Vac. Sci. Technol. A* **6**, 2390 (1988).
9. G. S. Bales *et al.*, *Science* **249**, 264 (1990).
10. R. Cuerno and A.-L. Barabási, *Phys. Rev. Lett.* **74**, 4746 (1995); R. Cuerno *et al.*, *ibid.* **75**, 4464 (1995).
11. M. Navez, C. Sella, D. Chaperot, *C. R. Acad. Sci.* **254**, 240 (1962).
12. S. W. MacLaren, J. E. Baker, N. L. Finnegan, C. M. Loxton, *J. Vac. Sci. Technol. A* **10**, 468 (1992).
13. G. Carter, M. J. Nobes, H. Stoere, I. V. Katardjiev, *Surf. Interface Anal.* **20**, 90 (1993).
14. The constant $D = D_s \gamma \Omega^2 n/k_B T$, where D_s is the

surface diffusion constant, Ω the atomic volume, ν the area density of diffusing surface atoms, γ the surface free energy, k_B the Boltzmann constant, and T the temperature (8).

15. I. Koponen, M. Hautala, O.-P. Sievänen, *Phys. Rev. Lett.* **78**, 2612 (1997).
16. Regular dots with a diameter of 50 nm are observed on InSb(100) surfaces after an exposure time of 100 s to Ar⁺ ions with an energy of 450 eV. On Ge(111) surfaces dots with a diameter of 16 nm could be

observed after an Ar⁺ ion exposure time of 1000 s with an ion energy of 1000 eV.

17. We thank D. Meertens and M. Feuerbacher (Institut für Festkörperforschung, Forschungszentrum Jülich, Germany) for the HTEM images and the energy-dispersive x-ray spectrometry analysis and C. Moormann (Advanced Microelectronic Center Aachen, Aachen, Germany) for the SEM pictures.

17 March 1999; accepted 9 July 1999

KDR Receptor: A Key Marker Defining Hematopoietic Stem Cells

B. L. Ziegler,*¹ M. Valtieri,*^{2,3} G. Almeida Porada,⁴
R. De Maria,^{2,3} R. Müller,¹ B. Masella,² M. Gabbianelli,³
I. Casella,² E. Pelosi,³ T. Bock,¹ E. D. Zanjani,⁴ C. Peschle^{2,3,†}

Studies on pluripotent hematopoietic stem cells (HSCs) have been hindered by lack of a positive marker, comparable to the CD34 marker of hematopoietic progenitor cells (HPCs). In human postnatal hematopoietic tissues, 0.1 to 0.5% of CD34⁺ cells expressed vascular endothelial growth factor receptor 2 (VEGFR2, also known as KDR). Pluripotent HSCs were restricted to the CD34⁺KDR⁺ cell fraction. Conversely, lineage-committed HPCs were in the CD34⁺KDR⁻ subset. On the basis of limiting dilution analysis, the HSC frequency in the CD34⁺KDR⁺ fraction was 20 percent in bone marrow (BM) by mouse xenograft assay and 25 to 42 percent in BM, peripheral blood, and cord blood by 12-week long-term culture (LTC) assay. The latter values rose to 53 to 63 percent in LTC supplemented with VEGF and to greater than 95 percent for the cell subfraction resistant to growth factor starvation. Thus, KDR is a positive functional marker defining stem cells and distinguishing them from progenitors.

The hierarchy of human hematolymphopoietic cells is defined by functional assays. HSCs with extensive self-renewal capacity are assayed in vivo for their capacity to xenograft nonobese diabetic-severe combined immunodeficiency disease (NOD-SCID) mice and sheep fetuses (1–3). These models are surrogates for a syngeneic transplantation assay. Primitive HPCs with limited self-renewal potential are identified in vitro as high-proliferative potential colony-forming cells (HPP-CFCs) (4). Lineage-committed HPCs with no self-renewal activity are also defined in vitro by clonogenic assays as colony-forming units (CFUs) or burst-forming units (BFUs) (1, 5). Dexter-type LTC, consisting of a liquid phase on irradiated BM stroma, identifies LTC-initiating cells (LTC-ICs, gener-

ating HPCs assayed in secondary culture) (6) and cobblestone area-forming cells (CAFCs, generating hematopoietic colonies recognized as “cobblestone areas” in LTC stroma) (7). Depending on the LTC duration, LTC-ICs represent primitive HPCs (5- to 8-week LTC) (8) or highly quiescent putative HSCs resistant to retroviral gene transfer (12-week LTC) (9) (see below).

Although HSC identification is still elusive, recent observations have suggested a role for VEGFR2 (Flk1 in mice) in murine embryonic hematopoiesis. Targeted gene disruption studies indicate that Flk1 is required for initiation of hematolymphopoiesis and vasculogenesis (10), implying that Flk1 may be required for generation of hemoangioblasts, that is, the hypothetical stem cells for both hematolymphopoietic and endothelial lineages (11). Other studies also suggested the existence of embryonic Flk1⁺ cells with hemoangiogenic potential but did not allow identification of prenatal repopulating HSCs (12). We identified KDR as a major functional marker for postnatal HSCs.

In postnatal life, KDR is expressed on endothelial cells (13), and the mRNA can be detected in HPCs and megakaryocytes (14, 15). We used a high-affinity monoclonal antibody (mAb clone 260.4) that binds the extracellular

¹Department of Hematology and Oncology, University of Tübingen, Otfried-Müller-Strasse 10, D-72076 Tübingen, Germany. ²Kimmel Cancer Institute, Thomas Jefferson University, 233 South 10 Street, Philadelphia, PA 19107-5541, USA. ³Department of Hematology and Oncology, Istituto Superiore di Sanità, V. le Regina Elena 299, 00161 Rome, Italy. ⁴Department of Veterans Affairs, University of Nevada, Reno, NV 89520, USA.

*These authors contributed equally to this work.
†To whom correspondence should be addressed. E-mail: cesare.peschle@mail.tju.edu

REPORTS

KDR domain to monitor KDR expression by flow cytometry on cells from BM, normal peripheral blood (PB) or mobilized peripheral blood (MPB), and cord blood (CB) (16). Only 0.1 to 0.5% of CD34⁺ cells \geq 95% pure from these tissues were KDR⁺ (Fig. 1A, top), as confirmed by reverse transcriptase polymerase chain reaction (RT-PCR) analysis (Fig. 1A, bottom right). The CD34⁺KDR⁺ cells, essentially lin⁻ (<10% CD45RA⁺; <5% CD13⁺, CD33⁺, CD61⁺, and CD19⁺), are at least in part positive for early progenitor and stem cell markers, namely, CD38⁻, Thy-1⁺, and kit^{low} (Fig. 1B). The published HSC-enriched fractions (for example, CD34⁺38⁻, CD34⁺Thy-1⁺, and CD34⁺ kit^{low}; see below) comprise \leq 1 to 2% of KDR⁺ cells.

VEGF treatment of human HPC culture or normal mice inhibits or stimulates hematopoiesis (17), possibly through growth factor (GF) release by accessory cells. In our studies, VEGF addition in 90 to 95% purified HPC culture (18) mildly stimulated multipotent CFU (CFU-Mix), HPP-CFCs, and LTC-ICs (19). Thereafter, we purified CD34⁺ cells and separated CD34⁺KDR⁺ versus CD34⁺KDR⁻ fractions (Fig. 1A, bottom left) (16). Both subsets were functionally analyzed. Upon addition of different GF combinations (20), we observed that PB lineage-committed HPCs (BFU-E and CFU-GM) were essentially restricted to the KDR⁻ fraction (Fig. 2A, left). Similar results were obtained for BM and CB (19). HPP-CFCs were

present in both KDR⁺ and KDR⁻ fractions. Their frequency in secondary cultures was more elevated in the former population (Fig. 2A, right). Similar results were obtained for BM and CB (19). In Dexter-type LTC (Fig. 2B), we evaluated the HPCs generated by LTC-ICs in 5-, 8- and 12-week LTC seeded with PB (Fig. 2B, left panel), BM, MPB, and CB cells (19). In CD34⁺ cell LTC, HPC production declined from the fifth through twelfth weeks; in KDR⁻ LTC, HPC production similarly declined at 5 to 8 weeks, but no residual HPCs were detected at 12 weeks. Conversely, in KDR⁺ LTC, the HPC number was low at 5 to 8 weeks but markedly increased at 12 weeks. An equivalent pattern was observed in BM, MPB, and CB LTC by 6-, 9- and 12-week CAFC assay (Fig. 2B, middle and right). Altogether, lineage-committed HPCs were restricted to KDR⁻ cells, whereas putative HSCs (12-week LTC-ICs and CAFCs) were restricted to KDR⁺ cells; the intermediate primitive HPCs (HPP-CFCs, 5- to 8-week LTC-ICs, 6- to 9-week CAFCs) were present in both fractions.

The frequency of putative HSCs was evaluated by limiting dilution analysis (LDA) (20). In VEGF-treated LTCs, the 12-week LTC-IC frequency was 0.19% in PB CD34⁺ cells [that is, one-sixth that of the more differentiated 5- to 8-week LTC-ICs (21)]. Twelve-week LTC-ICs were enriched by more than a factor of 300 in KDR⁺ fraction (63%) but absent in the KDR⁻ subset (Fig. 2C, top). Similar results were ob-

tained for BM and CB KDR⁺ cells by 12-week CAFC LDA (Fig. 2C, bottom). The LTC-IC and CAFC frequency in KDR⁺ fraction is significantly higher in VEGF⁺ (53 to 63%) than in VEGF⁻ (25 to 43%) LTC (Fig. 2C), suggesting a functional role for KDR in HSCs. Specifically, VEGF protected from apoptosis 20% of PB CD34⁺KDR⁺ cells seeded in single-cell culture in liquid phase serum-free GF⁻ medium (20) (Fig. 2D, top). The LTC-IC frequency in the starvation-resistant CD34⁺KDR⁺ subset was $>$ 95% (Fig. 2D, bottom).

To study repopulating HSCs, we transplanted irradiated NOD-SCID mice with CD34⁺ (50,000 to 250,000 per mouse), CD34⁺ KDR⁺ (5000 to 10,000 per mouse), and CD34⁺ KDR⁻ (10,000 to 250,000 per mouse) cells from BM, PB, MPB, or CB (22). The mice were not treated with cytokines and were killed after 3 months [the assay often involves cytokine treatment and usually lasts 1.5 to 2 months (8)]. BM, spleen, and PB were analyzed for human cells by flow cytometry with human-specific mAbs. We observed consistent engraftment with KDR⁺ or KDR^{+/±} cells and essentially no engraftment with the KDR⁻ fraction.

In a representative BM experiment (Fig. 3A), 250,000 CD34⁺ cells showed engraftment, whereas 250,000 double-sorted KDR⁻ cells did not (Fig. 3A, top left). KDR⁺ cells (100 to 1600) consistently engrafted the hematopoietic lineages (CD33⁺CD15⁺ and CD14⁺

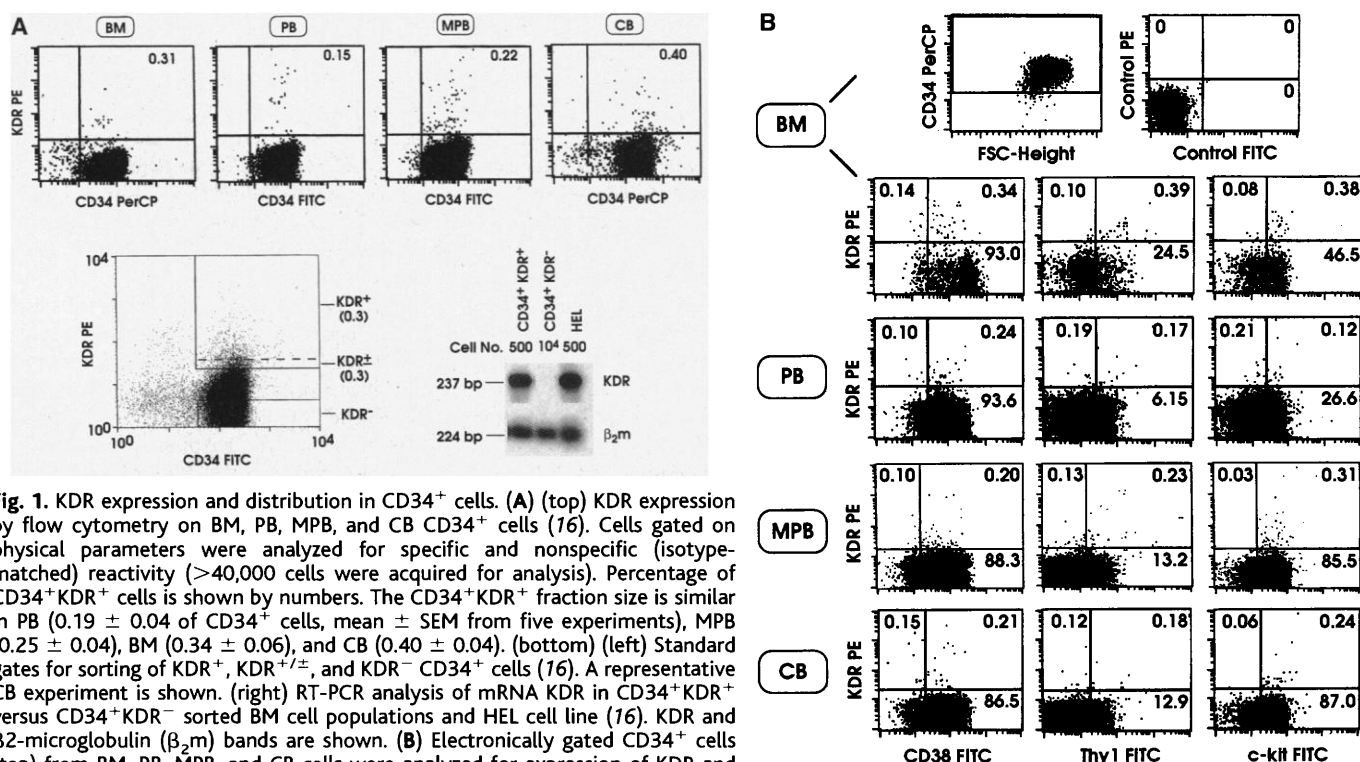


Fig. 1. KDR expression and distribution in CD34⁺ cells. (A) (top) KDR expression by flow cytometry on BM, PB, MPB, and CB CD34⁺ cells (16). Cells gated on physical parameters were analyzed for specific and nonspecific (isotype-matched) reactivity ($>$ 40,000 cells were acquired for analysis). Percentage of CD34⁺KDR⁺ cells is shown by numbers. The CD34⁺KDR⁺ fraction size is similar in PB (0.19 \pm 0.04 of CD34⁺ cells, mean \pm SEM from five experiments), MPB (0.25 \pm 0.04), BM (0.34 \pm 0.06), and CB (0.40 \pm 0.04). (bottom) (left) Standard gates for sorting of KDR⁺, KDR^{+/±}, and KDR⁻ CD34⁺ cells (16). A representative CB experiment is shown. (right) RT-PCR analysis of mRNA KDR in CD34⁺KDR⁺ versus CD34⁺KDR⁻ sorted BM cell populations and HEL cell line (16). KDR and β 2-microglobulin (β ₂m) bands are shown. (B) Electronically gated CD34⁺ cells (top) from BM, PB, MPB, and CB cells were analyzed for expression of KDR and relevant early hematopoietic antigens (16). CD34⁺KDR⁺ fraction cells are CD38⁻ (35.3% \pm 1.6 to 45.6% \pm 1.5 of cells, mean \pm SEM from four experiments), Thy-1⁺ (55.6% \pm 3.7 to 83.1% \pm 1.7), and kit^{low} (c-kit) (81.5% \pm 2.0 to 91.0% \pm 1.6, except for PB).

REPORTS

CD45⁺, CD71⁺GPA⁺, and CD45⁺ CD41⁺ cells in granulomonocytic, erythroid, and megakaryocytic series, respectively; Fig. 3A, bottom) and the B and T lymphoid compartments (CD19⁺CD20⁺ and CD4⁺CD8⁺CD3⁺, respectively) and natural killer (NK) cells (CD16⁺CD56⁺; Fig. 3A, bottom). A dose response was observed for all engrafted cell populations, specifically CD45⁺ cells (Fig. 3A, top right). Although T cell precursors require specific cognate interaction for maturation, human CD3⁺CD4⁺CD8⁺ and CD3⁺CD2⁺ cells have been generated in NOD-SCID mice BM after injection of CD34⁺CD38⁻ (2, 23) or CD34⁻lin⁻ cells (24). The in vitro BM microenvironment is permissive for T cell development and may recapitulate thymic maturation (25). Human T cell precursors may thus develop in NOD-SCID mice BM. The presence of contaminant mature T cells in the transplanted CD34⁺KDR⁺ cells can be excluded, in view of the lack of human T lymphocytes in mice re-

ceiving large numbers of CD34⁺KDR⁻.

After injection of 5 to 250 BM KDR⁺ cells, a dose-dependent multilineage engraftment was monitored (Fig. 3B). All mice were repopulated by 250 and 50 cells, whereas five of six and four of six mice injected with ten and five cells, respectively, were engrafted, on the basis of flow cytometry analysis (Fig. 3B, top left) and HPC assay validated by PCR of human alpha satellite DNA in the scored colonies (Fig. 3B, bottom). LDA indicated 20% of repopulating HSCs in CD34⁺KDR⁺ cells (Fig. 3B, top right). This value is similar to the LTC-IC and CAFC frequency in VEGF⁻ BM LTC (see above), indicating that repopulating HSCs and 12-week LTC-ICs and CAFCs are closely related. Because CAFC and LTC-IC frequency rose from 25 to 42% in VEGF⁻ to 53 to 63% in VEGF⁺ LTC, the repopulating HSC frequency may similarly rise in VEGF-treated mice.

CB cells (200 to 10,000 CD34⁺KDR⁺ or 10,000 to 200,000 CD34⁺KDR⁻ CB cells)

were xenotransplanted into NOD-SCID mice in five independent experiments. Human cells were virtually absent in mice transplanted with double-sorted KDR⁻ cells. In contrast, KDR⁺ cells consistently generated human CD45⁺ cells in BM, PB, and spleen in a dose-dependent pattern [for example, mice receiving 1000 to 10,000 cells showed 27.2 ± 7.1% (mean ± SEM) human CD45⁺ BM cells, whereas animals treated with 200 to 800 cells showed 3.75 ± 1.5% CD45⁺ BM cells]. In a representative experiment, mice transplanted with 6000 CD34⁺KDR⁺ cells (Fig. 3C) showed in BM abundant human CD34⁺ progenitors; precursors of the erythroid, granulomonocytic, and megakaryocytic lineages; and B and NK cells. The modest CD3 expression may reflect the low T cell generation potential of CB HSCs.

Repopulating HSCs were also assayed in fetal sheep (26–28). In a representative experiment, CD34⁺ cells were purified from two BM samples. The CD34⁺ population and

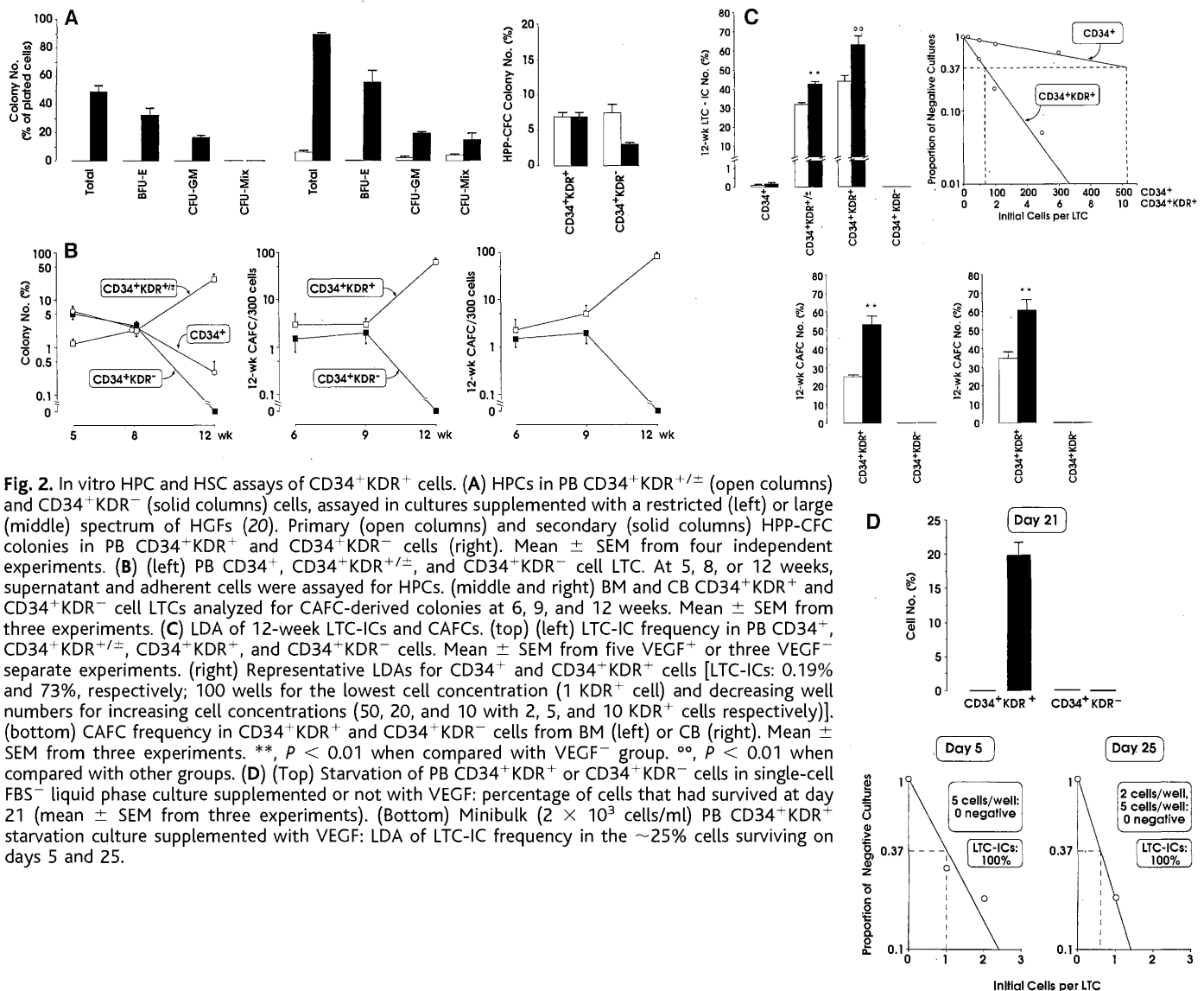


Fig. 2. In vitro HPC and HSC assays of CD34⁺KDR⁺ cells. (A) HPCs in PB CD34⁺KDR^{+/±} (open columns) and CD34⁺KDR⁻ (solid columns) cells, assayed in cultures supplemented with a restricted (left) or large (middle) spectrum of HGFs (20). Primary (open columns) and secondary (solid columns) HPP-CFC colonies in PB CD34⁺KDR⁺ and CD34⁺KDR⁻ cells (right). Mean ± SEM from four independent experiments. (B) (left) PB CD34⁺, CD34⁺KDR^{+/±}, and CD34⁺KDR⁻ cell LTC. At 5, 8, or 12 weeks, supernatant and adherent cells were assayed for HPCs. (middle and right) BM and CB CD34⁺KDR⁺ and CD34⁺KDR⁻ cell LTCs analyzed for CAFC-derived colonies at 6, 9, and 12 weeks. Mean ± SEM from three experiments. (C) LDA of 12-week LTC-ICs and CAFCs. (top) (left) LTC-IC frequency in PB CD34⁺, CD34⁺KDR^{+/±}, CD34⁺KDR⁺, and CD34⁺KDR⁻ cells. Mean ± SEM from five VEGF⁺ or three VEGF⁻ separate experiments. (right) Representative LDAs for CD34⁺ and CD34⁺KDR⁺ cells [LTC-ICs: 0.19% and 73%, respectively; 100 wells for the lowest cell concentration (1 KDR⁺ cell) and decreasing well numbers for increasing cell concentrations (50, 20, and 10 with 2, 5, and 10 KDR⁺ cells respectively)]. (bottom) CAFC frequency in CD34⁺KDR⁺ and CD34⁺KDR⁻ cells from BM (left) or CB (right). Mean ± SEM from three experiments. **, *P* < 0.01 when compared with VEGF⁻ group. °°, *P* < 0.01 when compared with other groups. (D) (Top) Starvation of PB CD34⁺KDR⁺ or CD34⁺KDR⁻ cells in single-cell FBS⁻ liquid phase culture supplemented or not with VEGF: percentage of cells that had survived at day 21 (mean ± SEM from three experiments). (Bottom) Minibulk (2 × 10³ cells/ml) PB CD34⁺KDR⁺ starvation culture supplemented with VEGF: LDA of LTC-IC frequency in the ~25% cells surviving on days 5 and 25.

REPORTS

the CD34⁺KDR^{+/-} versus CD34⁺KDR⁻ fractions were then injected in the fetuses of eight pregnant sheep. Primary recipients receiving KDR^{+/-}, KDR⁻, or unseparated CD34⁺ cells (four, three, and two fetuses per group, respectively) were killed on day 60 after transplant. Human CD34⁺ cells from primary fetuses treated with KDR^{+/-} cells were transplanted into secondary fetuses. Other fetuses injected with KDR^{+/-} or KDR⁻ cells were born.

In primary recipients, transplantation of CD34⁺ cells (1.2×10^5 per fetus) consistently induced engraftment. BM analysis indicated the presence of differentiated (0.30% CD45⁺ cells, mean value) and undifferentiated (0.17% CD34⁺ cells) human hematopoietic precursors; in clonogenic assay, 6.8% of CFU-Mix/BFU-E and 5.2% of CFU-GM of all colonies were of human origin. A small number of KDR^{+/-} cells (3×10^3 per fetus) consistently engrafted with impressive multilineage expression for the differentiated compartments (1.78% CD45⁺, 0.16% GPA⁺, and 0.34% CD3⁺ cells) and the undifferentiated one (0.32% CD34⁺ cells; the human HPC frequency was elevated, that is,

9.3% CFU-Mix and BFU-E and 16.2% CFU-GM). Eighty times as many KDR⁻ cells (2.4×10^5 per fetus) did not engraft, as indicated by consistent absence of CD34⁺ and CD3⁺ cells; only a few differentiated hematopoietic precursors were detected (0.7% CD45⁺ cells), together with a few late CFU-GM (2.4%) giving rise to small colonies. We estimated that a total of $>10^8$ CD34⁺ and CD3⁺ human cells were generated per fetus by KDR⁺ cells, whereas no CD34⁺ and CD3⁺ cells were generated by KDR⁻ cells (Fig. 4, top and middle).

Four secondary recipients received human BM CD34⁺ cells, derived from primary fetuses treated with KDR^{+/-} cells. After 2 months the secondary recipients were killed and showed multilineage engraftment (Fig. 4, bottom).

At 3 weeks after birth, both sheep transplanted with KDR⁺ cells in fetal life showed persistent multilineage engraftment at BM level. One sheep featured extremely abundant human CD45⁺ cells (23.9%). Conversely, the sheep transplanted with KDR⁻ cells showed no engraftment.

These fetal sheep results, confirmed in other

experiments, indicate that the KDR⁺ fraction is enriched for HSCs giving rise to multilineage engraftment in primary, secondary, and born recipients. Positive results in secondary recipients successfully compare with those observed by follow-up of primary transplanted fetuses for long periods after birth (28). Conversely, the KDR⁻ fraction does not engraft and contains only HPCs giving rise in primary recipients to differentiated precursors and a few late CFU-GM.

The in vivo assay results indicate HSC restriction to the KDR⁺ subfraction of CD34⁺ cells, thus in line with the in vitro observations. Previous studies in NOD-SCID mice and fetal sheep showed that HSCs are enriched in diverse CD34⁺ cell subfractions [CD38⁻ (2, 23, 27), kit^{low}, Thy-1⁺, or Rhodamine (Rho)^{dim} (28)], but engraftment was also observed at lower level for the complementing subfractions [that is, CD38⁺ (2, 23, 27), kit⁻, Thy-1⁻, or Rho^{bright} (28)].

In conclusion, HSCs are in the CD34⁺KDR⁺ cell fraction, whereas lineage-committed HPCs are restricted to the CD34⁺KDR⁻ subset. The 20% repopulating HSC frequency

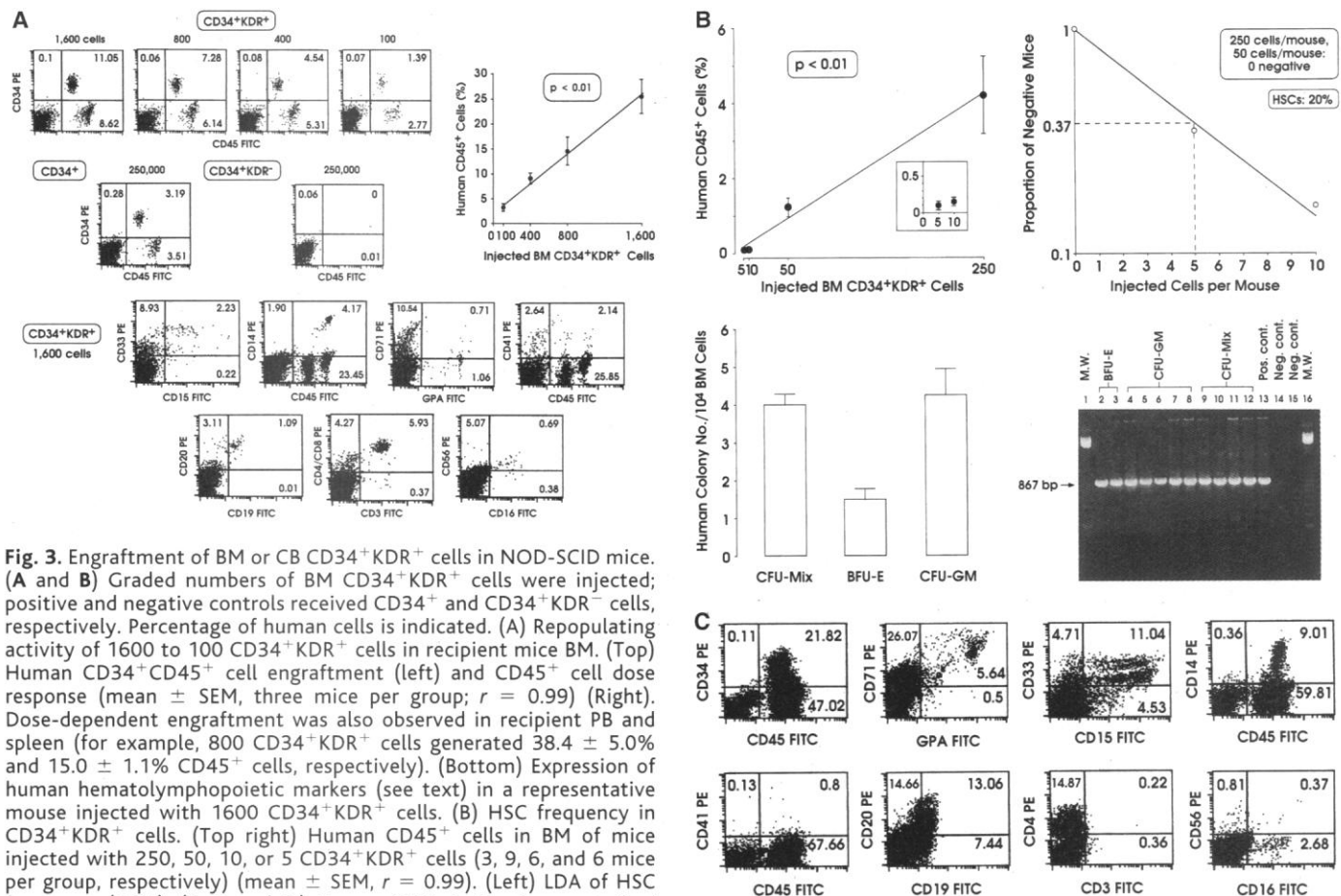
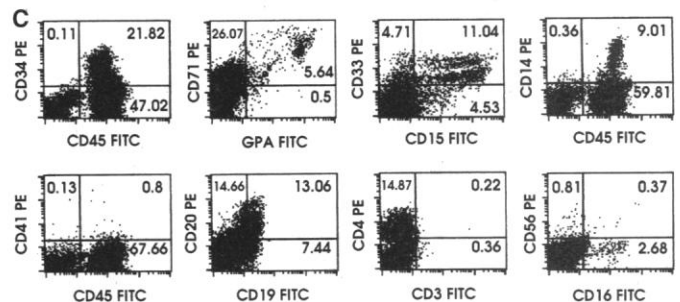
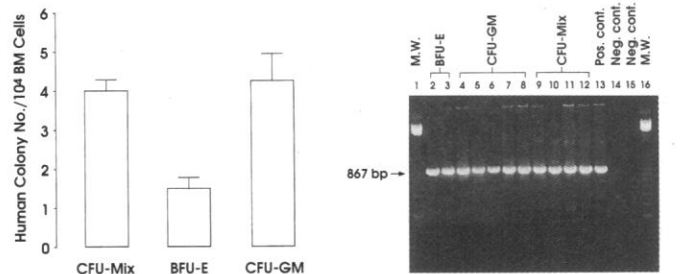


Fig. 3. Engraftment of BM or CB CD34⁺KDR⁺ cells in NOD-SCID mice. (A and B) Graded numbers of BM CD34⁺KDR⁺ cells were injected; positive and negative controls received CD34⁺ and CD34⁺KDR⁻ cells, respectively. Percentage of human cells is indicated. (A) Repopulating activity of 1600 to 100 CD34⁺KDR⁺ cells in recipient mice BM. (Top) Human CD34⁺CD45⁺ cell engraftment (left) and CD45⁺ cell dose response (mean \pm SEM, three mice per group; $r = 0.99$) (Right). Dose-dependent engraftment was also observed in recipient PB and spleen (for example, 800 CD34⁺KDR⁺ cells generated $38.4 \pm 5.0\%$ and $15.0 \pm 1.1\%$ CD45⁺ cells, respectively). (Bottom) Expression of human hematopoietic markers (see text) in a representative mouse injected with 1600 CD34⁺KDR⁺ cells. (B) HSC frequency in CD34⁺KDR⁺ cells. (Top right) Human CD45⁺ cells in BM of mice injected with 250, 50, 10, or 5 CD34⁺KDR⁺ cells (3, 9, 6, and 6 mice per group, respectively) (mean \pm SEM, $r = 0.99$). (Left) LDA of HSC frequency (20%). (Bottom left) Human HPCs in the four engrafted mice injected with five cells (mean \pm SEM). (Right) PCR analysis of alpha satellite DNA [867-base pair (bp) band] in all scored colonies from a representative mouse in the five-cell group (lane 13, human DNA positive control; lane 14, no template control; lane 15,



DNA from BM mononuclear cells of nontransplanted mouse; M.W., molecular weight marker). (C) A representative mouse receiving 6000 CB CD34⁺KDR⁺ cells: informative human hematopoietic markers (see text).

in CD34⁺KDR⁺ BM fraction is >100 times as elevated as that in CD34⁺38⁻ BM or CB cells (2), as confirmed in our laboratory (19). This difference is readily predicted by comparing HSC activity and phenotype. Because CD34⁺KDR⁻ cells do not comprise HSCs but represent 98 to 99% of CD34⁺CD38⁻ cells (Fig. 1B), it follows that the HSC frequency in CD34⁺CD38⁻ cells is far lower (that is, <2%) than that in CD34⁺KDR⁺ cells. The VEGF effects on CD34⁺KDR⁺ cells suggest that KDR plays a functional role in HSCs. Preliminary observations indicate that transfer of Flk1 gene into PB CD34⁺KDR⁻ cells partially rescues the HSC phenotype (19).

Large numbers (≥10⁵) of BM or CB CD34⁺lin⁻ cells engraft fetal sheep and NOD-SCID mice with multilineage hematopoietic expression (3, 24). We observed in BM and CB that ≤1% CD34⁺lin⁻ cells are KDR⁺ (29), the total number of CD34⁺lin⁻KDR⁺ cells was ≤50% that of CD34⁺KDR⁺ cells, and a discrete number of CD34⁺lin⁻KDR⁺ cells engrafted NOD-SCID mice with multilineage expression, but the relative stem cell activity of

the CD34⁺KDR⁺ fraction is more elevated. The stem cell activity in the CD34⁺KDR⁺ fraction was predominant, in line with studies indicating that human HSCs with long-term engraftment capacity are CD34⁺ (30).

Murine studies suggested that embryonic Flk1⁺ cells have hemoangiogenic potential but did not identify prenatal repopulating HSCs (10, 12). Our observations in humans identify postnatal CD34⁺KDR⁺ and CD34⁻KDR⁺ repopulating HSCs. The CD34⁻KDR⁺ and CD34⁺KDR⁺ phenotypes might define the postnatal and prenatal HSC-hemoangioblast.

Purification of CD34⁺ HPCs has facilitated studies on early hematopoiesis (1, 5). Isolation of KDR⁺ HSCs offers an opportunity to elucidate the cellular and molecular phenotype and functional properties of HSCs and HSC subsets. These issues are of pivotal importance for a large array of biotechnological and clinical challenges, such as HSC transplantation, in vitro blood cell generation for transfusion, and HSC gene therapy.

References and Notes

1. M. Ogawa, *Blood* **81**, 2844 (1993).
2. M. Bhatia, J. C. Y. Wang, U. Kapp, D. Bonnet, J. E. Dick, *Proc. Natl. Acad. Sci. U.S.A.* **94**, 5320 (1997); J. C. Y. Wang, M. Doedens, J. E. Dick, *Blood* **89**, 3919 (1997); E. Conneally, J. Cashman, A. Petzer, C. Eaves, *Proc. Natl. Acad. Sci. U.S.A.* **94**, 9836 (1997).
3. E. D. Zanjani, G. Almeida-Porada, A. G. Livingston, A. W. Flake, M. Ogawa, *Exp. Hematol.* **26**, 353 (1998).
4. J. Brandt, E. F. Srouf, K. van Besien, R. A. Briddell, R. Hoffman, *J. Clin. Invest.* **86**, 932 (1990).
5. M. Gabbianelli et al., *Science* **249**, 1561 (1990).
6. H. J. Sutherland, P. M. Lansdorp, D. H. Henckelman, A. C. Eaves, C. J. Eaves, *Proc. Natl. Acad. Sci. U.S.A.* **87**, 3584 (1990).
7. J. C. van der Loo and R. E. Ploemacher, *Blood* **85**, 2598 (1995).
8. A. Larochelle et al., *Nature Med.* **2**, 1329 (1996).
9. Q. L. Hao, F. T. Thiemann, D. Petersen, E. M. Smogorzewska, G. M. Crooks, *Blood* **88**, 3306 (1996).
10. F. Shalaby et al., *Cell* **89**, 981 (1997).
11. W. Risau and I. Flamme, *Annu. Rev. Cell Dev. Biol.* **11**, 73 (1995); A. Eichmann et al., *Proc. Natl. Acad. Sci. U.S.A.* **94**, 5141 (1997).
12. N. Kabrun et al., *Development* **124**, 2039 (1997); M. Kennedy et al., *Nature* **386**, 488 (1997); S. I. Nishikawa, S. Nishikawa, M. Hirashima, N. Matsuyoshi, H. Kodama, *Development* **125**, 1747 (1998); K. Choi, M. Kennedy, A. Kazarov, J. C. Papadimitriou, G. Keller, *ibid.*, p. 725.
13. T. Asahara et al., *Science* **275**, 964 (1997).
14. O. Katoh, H. Tauchi, K. Kawaiishi, A. Kimura, Y. Satow, *Cancer Res.* **55**, 5687 (1995).
15. PB HPCs 90 to 95% pure were grown in unilineage differentiation cultures (31). RT-PCR analysis (16) indicated that KDR mRNA is expressed at low levels in HPCs but is not detected in the HPC progeny except megakaryocytes.
16. BM cells were obtained from consenting normal donors. MPB was obtained from G-CSF-treated (5 mg/kg) consenting normal donors. Normal PB was collected as buffy coat preparation from the local blood bank. CB was obtained from healthy, full-term placentas according to institutional guidelines. Low-density cells (<1.077 g/ml) were isolated by Ficoll and CD34⁺ cells purified by MiniMACS column (Miltenyi Bergisch Gladbach, Germany). Purified CD34⁺ cells were incubated for 30 min on ice with saturating amounts of biotinylated anti-KDR mAb (done 260.4; Gesellschaft für Biologische Forschung, Braunschweig, Germany) and anti-CD34 fluorescein isothiocyanate (FITC) mAbs (clone HPCA-2; Becton-Dickinson, San

Jose, CA). For three-color FACS analysis, anti-CD34 PerCP and one of the following FITC-conjugated mAbs was used: anti-CD38 (Becton-Dickinson), anti-flt3 (Immunotech, Marseille, France), anti-Thy-1 (Pharmingen, San Diego, CA), and anti-c-kit (Serotec, Oxford, UK). Cells were then washed and labeled with streptavidin-phycoerythrin (PE) (Becton-Dickinson). After a further washing, cells were run on a FACScan or FACSCalibur for two- or three-color analysis. Purified CD34⁺ cells were incubated with saturating amounts of anti-CD34-FITC and biotinylated anti-KDR, washed, and labeled with streptavidin-PE. After a further washing, CD34⁺KDR⁺ or KDR⁺ and CD34⁺KDR⁻ subpopulations were sorted on FACSVantage (Becton-Dickinson) or EPICS Elite (Coulter) (fluorescence emission, 525 and 575 nm). A fraction of sorted KDR⁻ cells was reanalyzed. If contaminating KDR⁺ cells were detected, the population was retained and resorted to ensure elimination of all KDR⁺ cells. KDR RT-PCR was performed as described (32) with 5'-AAAACCTTTTGTGCTTTT-TGA-3' and 5'-GAAATGGGATTGTAAGGATGA-3' primers (33).

17. E. Broxmeyer et al., *Int. J. Hematol.* **62**, 203 (1995); D. Gabrilovich et al., *Blood* **92**, 4150 (1998).
18. M. Gabbianelli et al., *Blood* **86**, 1661 (1995).
19. B. L. Ziegler et al., data not shown.
20. In the HPC assay, cells were seeded in 0.9% methylcellulose fetal bovine serum-free (FBS⁻) medium supplemented with saturating amounts of GFs (flt3 ligand (FL), kit ligand (KL), basic fibroblast GF (bFGF) (100 ng/ml each), interleukin-6 (IL-6) (10 ng), IL-3 (100 U), granulomonocyte colony-stimulating factor (GM-CSF) (10 ng), G-CSF (500 U), M-CSF (250 U), thrombopoietin (Tpo) (100 ng), and erythropoietin (Epo) (3 U)). CFU-Mix-BFU-E and CFU-GM colonies comprised >5 × 10³ and >10³ cells respectively (18). A more limited GF combination comprised IL-3, GM-CSF, and Epo at the indicated dosages (18) [this culture condition was also used for NOD-SCID mice BM mononuclear cell (MC) clonogenesis]. CFU-Mix-BFU-E and CFU-GM colonies comprised >500 and 100 cells, respectively. For detection of human colonies, the colony DNA was processed for PCR with KlenTaq-1 DNA polymerase (Clontech, Palo Alto, CA) and primers recognizing human alpha satellite sequences on chromosome 17 (34). In the HPP-CFC assay (18), primary HPP-CFC clones, scored at day 30, were replated for secondary HPP-CFC colony formation. Five-, 8-, and 12-week LTCs were established on allogeneic irradiated [20 grays (Gy)] BM stromas (18) or FBMD-1 cells (7). At weekly intervals, half of the medium was removed and replaced by fresh medium ± VEGF (100 ng/ml). In 12-week LTC, irradiated BM stromas or fresh FBMD-1 cells were added monthly to prevent functional exhaustion of the initial inoculum (9). In minibulk LTC, each well was seeded with 100 to 1000 CD34⁺KDR⁺ cells (1000 cells/ml) (positive or negative control was seeded with 10,000 CD34⁺ or CD34⁺KDR⁻ cells, respectively). LTCs were terminated at 5, 8, or 12 weeks. Cells from supernatant and adherent fractions were cultured in semisolid medium for colony growth (18). Alternatively, 6-, 9-, and 12-week CAFCs were scored directly in LTC adherent layer (7). In LDA studies, graded numbers of CD34⁺KDR⁺ cells were seeded in LTC wells (6, 27) (see figure legends). The frequency of 12-week LTC-ICs and CAFCs was calculated according to single-hit Poisson statistics (6, 27). Control LDA was performed on CD34⁺KDR⁻ cells (10 to 5000 cells per well) and unseparated CD34⁺ cells (20 to 5000 cells per well). Liquid phase suspension culture in FBS⁻ medium ± VEGF (100 ng/ml) was performed as in (32).
21. A. Carè et al., *Oncogene* **18**, 1993 (1999).
22. Six- to 8-week-old mice (Jackson Laboratory, Bar Harbor, ME) were irradiated at 3.5 Gy with a ¹³⁷Cs source (Gammacell) 12 to 24 hours before xenotransplantation. KDR⁺ or KDR⁻ cells were injected intravenously together with 100,000 irradiated (20 Gy) BM or CB MCs into the lateral tail vein. Mice were killed 12 weeks after xenotransplantation according to institutional regulations. Cell suspensions from femurs, spleen, and PB were analyzed for human cells by flow cytometry. Erythrocyte-depleted cells were

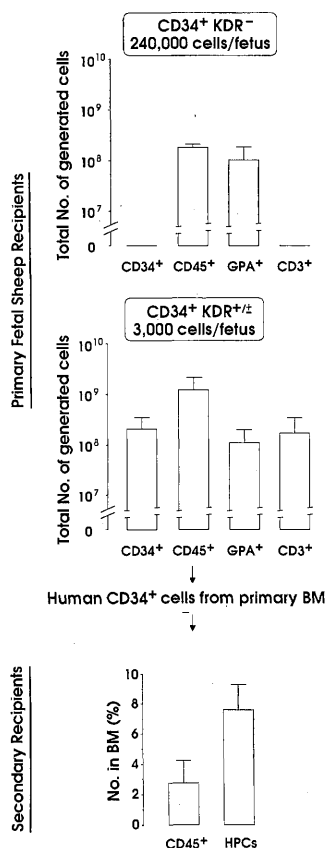


Fig. 4. Engraftment of BM CD34⁺KDR⁺ cells in fetal sheep. Total number of human CD34⁺, CD45⁺, GPA⁺, and CD3⁺ cells generated in primary fetuses injected with CD34⁺KDR⁺ or CD34⁺KDR⁺/± cells (top and middle, mean ± SEM). Human CD45⁺ cells and HPCs in BM of secondary fetuses (bottom, mean ± SEM), each injected with 4 × 10⁵ human CD34⁺ cells from BM of primary fetuses.

labeled with FITC- or PE-conjugated mAbs directed against the following markers: CD45 (HLc1), CD34 (HPCA-2), CD38, CD15, CD33, CD71, CD2, CD3, CD4, CD7, CD8, CD19, CD20, CD16, CD56 (Becton-Dickinson), GPA, and CD71 (Pharmingen). FITC- or PE-conjugated isotype-matched irrelevant mAbs were used as controls. BM, spleen, and PB cells from non-transplanted mice were used as negative control. Positive controls consisted of human BM or CB MCs. BM MCs were also cultured in semisolid media selective for human HPCs (20).

23. M. M. Versteegen *et al.*, *Blood* **91**, 1966 (1998).

24. M. Bhatia, D. Bonnet, B. Murdoch, O. I. Gan, J. E. Dick, *Nature Med.* **4**, 1038 (1998).

25. M. E. Garcia-Ojeda, S. Dejbakhsh-Jones, I. L. Weissman, S. Strober, *J. Exp. Med.* **187**, 1813 (1998).

26. For the fetal sheep xenografts (3, 27, 28), PB and BM MCs from chimeric fetuses or newborns, separated by Ficoll gradient, were evaluated for the presence of human cells by flow cytometry. BM MCs were also assayed for human HPCs in clonogenic culture by karyotyping of hematopoietic colonies. Human CD34⁺ cells, isolated by MiniMACS column from BM MCs (16), were transplanted in secondary recipients.

27. C. I. Civin *et al.*, *Blood* **88**, 4102 (1996).

28. I. Kawashima *et al.*, *ibid.* **87**, 4136 (1996); D. R. Sutherland *et al.*, *Exp. Hematol.* **24**, 795 (1996); N. Uchida *et al.*, *Blood* **88**, 1297 (1996).

29. CD34⁻lin⁻ cells were purified as in (24). The CD34⁻lin⁻KDR⁺ cell subfraction was analyzed and sorted as in (16).

30. R. J. Berenson *et al.*, *J. Clin. Invest.* **81**, 951 (1988); *Blood* **77**, 1717 (1991); W. I. Bensinger *et al.*, *ibid.* **88**, 4132 (1996); E. D. Zanjani, G. Almeida-Porada, A. W. Flake, *Int. J. Hematol.* **63**, 179 (1996).

31. U. Testa *et al.*, *Blood* **88**, 3391 (1996).

32. B. L. Ziegler *et al.*, *ibid.* **93**, 3355 (1999).

33. B. I. Terman *et al.*, *Oncogene* **6**, 1677 (1991).

34. P. E. Warburton, G. M. Greig, T. Haaf, H. F. Willard, *Genomics* **11**, 324 (1991)

3 February 1999; accepted 8 July 1999

Whole-Genome Shotgun Optical Mapping of *Deinococcus radiodurans*

Jieyi Lin,^{1*} Rong Qi,¹ Christopher Aston,^{1†} Junping Jing,^{1‡} Thomas S. Anantharaman,² Bud Mishra,² Owen White,³ Michael J. Daly,⁴ Kenneth W. Minton,⁴ J. Craig Venter,⁵ David C. Schwartz^{1,2§}

A whole-genome restriction map of *Deinococcus radiodurans*, a radiation-resistant bacterium able to survive up to 15,000 grays of ionizing radiation, was constructed without using DNA libraries, the polymerase chain reaction, or electrophoresis. Very large, randomly sheared, genomic DNA fragments were used to construct maps from individual DNA molecules that were assembled into two circular overlapping maps (2.6 and 0.415 megabases), without gaps. A third smaller chromosome (176 kilobases) was identified and characterized. Aberrant nonlinear DNA structures that may define chromosome structure and organization, as well as intermediates in DNA repair, were directly visualized by optical mapping techniques after γ irradiation.

Detailed, structural knowledge of whole microbial genomes is of primary importance to many genomic studies, but this information has been difficult to obtain. Pulsed-field gel electrophoresis (PFGE) plus Southern (DNA) blot analysis (1) provides primary genome information but does not confidently size large circular genomes and frequently ob-

scures the analysis of large episomal elements. Although an eight-enzyme restriction map of the *Escherichia coli* K12 genome was constructed in 1987 by Kohara *et al.* (2), this required a laborious approach involving partial digestion of 3400 phage clones followed by Southern blot analysis. Physical maps of the *Saccharomyces cerevisiae* genome were also prepared by painstaking restriction mapping of clones (3). Modern microbial genome analysis uses shotgun sequencing, followed by finishing efforts (4, 5). Whole-genome restriction maps may become an indispensable resource for large-scale genome sequencing projects. They facilitate sequence assembly by providing a scaffold for high-resolution alignment and verification of sequence assemblies (contigs), accurate genome sizing, and discernment of extrachromosomal elements (6).

Optical mapping is a system for the construction of ordered restriction maps from individual DNA molecules (7, 8) and has been used to prepare restriction maps of a number of clone types, including phage clones (9), yeast artificial chromosomes (10), bacterial artificial chromosomes (6), and, more recently, an entire electrophoretically

separated chromosome (~1 Mb) from *Plasmodium falciparum* (11). An optical mapping approach for whole bacterial genome analysis is feasible because we can now mount and map extremely large, randomly sheared DNA molecules (0.4 to 2.4 Mb) that are digested with high cutting efficiency (70 to 90%). These parameters critically control the success rate of assembling the fragments and are well modeled by prior probabilistic (Bayesian) analysis (12). The contigs covering a whole genome were initially assembled manually, or later with the Gentig algorithm (13), which automatically computes contigs of genomic maps.

To efficiently collect such large molecules, we developed a semiautomated image acquisition system that collects successive images and correctly assembles them into one large superimage while maintaining proper pixel registration between images. A new image analysis system was developed [Visionade (14)] that enables markup of molecular images, allows for editing, and automatically calculates fragment masses and cutting efficiencies. A λ bacteriophage DNA sizing standard was used as follows. First, the total integrated fluorescence intensity of the standard was determined to be in the correct range. Second, the size of each genomic fragment in a particular image was calculated by dividing the fluorescence intensity of the DNA fragment by the average fluorescence intensity of the standards in the image and then multiplying this by the size of the standard. The images were not used as data if the cutting efficiency along the length of the molecule was less than 75%.

The development of Gentig enabled the rapid assembly of raw maps into a complete genome-wide map in minutes rather than months, with negligible false positives. Contigs of the *E. coli* genome were assembled with Gentig into a consensus map, which both reproduced the map constructed by hand and correlated with the map predicted by sequence. Gentig automatically generates contigs from optical mapping data by repeatedly combining the two islands that produce the greatest increase in probability density, excluding any contigs whose false positive overlap probability is unacceptable. The stan-

¹W. M. Keck Laboratory for Biomolecular Imaging, Department of Chemistry, New York University, 31 Washington Place, New York, NY 10003, USA. ²Courant Institute of Mathematical Sciences, Department of Computer Science, New York University, 251 Mercer Street, New York, NY 10012, USA. ³The Institute for Genomic Research, 9712 Medical Center Drive, Rockville, MD 20850, USA. ⁴Uniformed Services University of the Health Sciences, Bethesda, MD 20814, USA. ⁵Celera Genomics, 45 West Gude Drive, Rockville, MD 20850, USA.

*Present address: Genome Therapeutics Corp., 100 Beaver Street, Waltham, MA 02154, USA.

†Present address: CNS Disorders, Wyeth-Ayerst Research, Princeton, NJ 08543, USA.

‡Present address: Smith Kline Beecham Pharmaceuticals, King of Prussia, PA 19406, USA.

§To whom correspondence should be addressed. Present address: Departments of Chemistry and Genetics, UW Biotechnology Center, University of Wisconsin, 425 Henry Mall, Madison, WI 53706, USA. E-mail: schwad01@mcrcr.med.nyu.edu